Biagioniite, Tl_2SbS_2, from the Hemlo gold deposit, Marathon, Ontario, Canada: occurrence and crystal structure

LUCA BINDI[1,2,*] and YVES MOËLO[3]

[1]Dipartimento di Scienze della Terra, Università degli Studi di Firenze, Via G. La Pira 4, I-50121 Firenze, Italy
[2]CNR-Istituto di Geoscienze e Georisorse, Sezione di Firenze, Via G. La Pira 4, I-50121 Firenze, Italy
[3]Université de Nantes, CNRS, Institut des Matériaux Jean Rouxel, IMN, F-44000 Nantes, France

* e-mail: luca.bindi@unifi.it

ABSTRACT

Biagioniite, ideally Tl_2SbS_2, is a new mineral from the Hemlo gold deposit, Marathon, Ontario, Canada. It occurs as very rare anhedral crystals up to 65 μm across associated with aurostibite, stibarsen and native gold in a calcite matrix. Biagioniite is opaque with a metallic luster and shows a black streak. In reflected light biagioniite is moderately bireflectant and not pleochroic. Under crossed polars it is weakly anisotropic with blueish to light-blue rotation tints. Internal reflections are absent. Reflectance percentages for the four COM wavelengths (R_{min} and R_{max}) are 35.9, 37.5 (471.1 nm), 34.7, 36.2 (548.3 nm), 33.8, 35.3 (586.6 nm), and 31.5, 33.7 (652.3 nm), respectively. A mean of 4 electron microprobe analyses gave Tl 65.12(31), Ag 3.52(9), Sb 20.22(12), S 10.80(8), total 99.66 wt%, corresponding, on the basis of a total of 5 atoms, to $(Tl_{1.87}Ag_{0.19})_{\Sigma 2.06}Sb_{0.97}S_{1.97}$. Biagioniite is

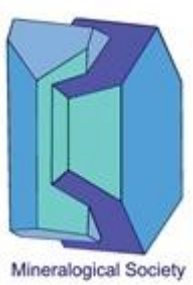

This is a 'preproof' accepted article for Mineralogical Magazine. This version may be subject to change during the production process.
DOI: 10.1180/mgm.2020.27

monoclinic, space group *Pc*, with a = 11.0895(9), b = 14.3124(11), c = 7.9352(6) Å, β = 96.230(8)°, V = 1252.02(17) Å^3 and Z = 8. The four strongest powder-diffraction lines [d in Å (I/I_0) (*hkl*)] are: 3.56 (100) (310); 3.37 (75) (-231); 3.79 (60) (012); 3.03 (60) (032). In the crystal structure [R_1 = 0.024 for 2655 reflections with $I > 2\sigma(I)$], thallium adopts various coordinations extending from quasi linear to quasi tetrahedral. Antimony forms Sb-Sb pairs, which lead to the formula $[Tl^{+1}]_4[Sb_2]^{4+}[S^{2-}]_4$. Biagioniite is isostructural with dervillite, Ag_2AsS_2. The new mineral has been approved by the IMA-CNMNC (No. 2019–120) and named for Cristian Biagioni, Associate Professor of Mineralogy at the Department of Earth Sciences of the University of Pisa, Italy.

Keywords: biagioniite, new mineral, thallium, sulfosalt, Hemlo deposit, Canada.

INTRODUCTION

Several elements, having economic value or environmental concern, are hosted in sulfosalts, a group of complex minerals typically occurring in hydrothermal settings. Our ongoing effort in the last two decades (Bindi and Biagioni, 2018, and references therein) has been the study of these minerals from a structural point of view to try to: *i*) elucidate the role played by minor components, which could give interesting insights into the physico-chemical conditions of the crystallization environments, and *ii*) allow the potential description of unpredictable structures, unexpected crystallographic features, and new mineral species. Such a body of knowledge has been critical for assessing both the technological potentialities of sulfosalts as well as their geological significance.

In the course of this research project (i.e., Biagioni *et al.*, 2016; Bindi *et al.*, 2012a, 2012b, 2015a, 2015b), we examined a sample from the Hemlo gold deposit, Marathon, Ontario, Canada (Harris, 1989), belonging to the mineralogical collections of the Museo di Storia Naturale of the University of Florence. The sample consists of tiny criddleite grains

closely associated with aurostibite, stibarsen and native gold in a calcite matrix. Among the stibarsen fragments, a small unique grain that turned out to be biagioniite, Tl_2SbS_2, was found.

Biagioniite was approved as a new mineral by the IMA-CNMNC (2019-120). The mineral name honours Cristian Biagioni (b. 1981), Associate Professor of Mineralogy at the Department of Earth Sciences of the University of Pisa, Italy. He is the current Italian Member of the IMA-Commission of New Minerals, Nomenclature and Classification and he is coauthor of the description of more than 50 new mineral species. In addition, he contributed to the discovery of the Tl-rich nature of pyrite ores from the Apuan Alps (northern Tuscany, Italy), promoting a new scientific investigations of these ore deposits both from a mineralogical and environmental point of view (e.g., Biagioni *et al.*, 2013, 2017). The holotype material is deposited in the mineralogical collection of the Museo di Storia Naturale of the University of Florence (Italy), under catalog number 46582/G.

Here we report the description of the new mineral biagioniite, together with the determination of its crystal structure.

MATERIAL STUDIED

The Museum sample containing biagioniite comes from the Hemlo gold deposit, which is located near the northeast shore of Lake Superior, 35 km east of Marathon, Ontario (Harris, 1989; Tomkins *et al.*, 2004). The deposit, discovered in 1982, is of Archean age and occurs at the contact of felsic metavolcanics and pelitic metasediments. It consists of several mineralized zones, of which the main zone extends for a length of 2900 m, for a distance of 2500 m down-dip and ranges in thickness from 3 to 45 m. The ore minerals were formed from hydrothermal fluids that may in part be related to the shear zone.

Native gold is the principal gold mineral in the deposit (Harris, 1989). The gold ore is substantially enriched in Mo, V, As, Sb, Hg, Tl and Ba and contains a diverse assemblage of minerals. Interestingly, there is a close spatial association between the mercury and thallium minerals. In this regard, the realgar-cinnabar-rich quartz veins that occur within the central portion of the deposit are common hosts for the thallium minerals (Harris, 1989). Routhierite is the most common thallium mineral, parapierrotite is less abundant, vaughanite and criddleite are rare.

PHYSICAL AND OPTICAL PROPERTIES

Biagioniite occurs as very rare crystals grown on a calcite matrix (Fig. 1). The mineral exhibits a subhedral to anhedral grain morphology, and does not show any inclusions of, or intergrowths with, other minerals. The maximum grain size of biagioniite is about 65 μm. It is black in colour and shows a black streak. The mineral is opaque in transmitted light and exhibits a metallic luster. No cleavage is observed, and the fracture is uneven. The calculated density (for Z = 8) for the empirical formula (see below) is 6.192 g/cm^3. Unfortunately, the density could not be measured here because of the small grain size. The Mohs hardness, estimated with respect to the surrounding calcite, is ~ 3.

In plane-polarized incident light, biagioniite is creamy in colour, moderately bireflectant and not pleochroic. Between crossed polars, biagioniite is weakly anisotropic with blueish to light-blue rotation tints. Internal reflections are absent and there is no optical evidence of growth zonation.

Reflectance measurements were performed in air by means of a MPM-200 Zeiss microphotometer equipped with a MSP-20 system processor on a Zeiss Axioplan ore microscope. The filament temperature was approximately 3350 K. An interference filter was adjusted, in turn, to select four wavelengths for measurement (471.1, 548.3, 586.6, and 652.3

nm). Readings were taken for specimen and standard (SiC) maintained under the same focus conditions. The diameter of the circular measuring area was 0.04 mm. Reflectance percentages for R_{min} and R_{max} are 35.9, 37.5 (471.1 nm), 34.7, 36.2 (548.3 nm), 33.8, 35.3 (586.6 nm), and 31.5, 33.7 (652.3 nm), respectively.

CHEMICAL COMPOSITION

A preliminary chemical analysis using EDS performed on the crystal fragment used for the structural study did not indicate the presence of elements (Z > 9) other than Tl, Sb and S, and minor Ag. Analyses were carried out using a JEOL 8200 microprobe (WDS mode, 25 kV, 20 nA, 1 μm beam size, counting times 20 s for peak and 10 s for background). The following lines were used: Ag *Lα*, Tl *Mα*, Sb *Lβ*, S *Kα*. The standards employed were: synthetic TlI (Tl), Ag-pure element (Ag), synthetic Sb_2Te_3 (Sb) and pyrite (S). The crystal fragment was found to be homogeneous within analytical error. The average chemical compositions (4 analyses on different spots) together with wt% ranges of elements are reported in Table 1. On the basis of 5 atoms, the empirical formula of biagioniite is $(Tl_{1.87}Ag_{0.19})_{\Sigma 2.06}Sb_{0.97}S_{1.97}$. The simplified ideal formula is $(Tl,Ag)_2SbS_2$, and the ideal formula is Tl_2SbS_2 (Z = 8), which requires Tl 68.74, Sb 20.48, S 10.78, Total 100 wt.%.

X-RAY CRYSTALLOGRAPHY AND CRYSTAL-STRUCTURE DETERMINATION

The same crystal fragment (40 × 50 × 65 μm) used to obtain the chemical data was selected for the X-ray single-crystal diffraction study that was done with a Bruker D8 Venture diffractometer equipped with an Photon II CCD detector, with graphite-monochromatized Mo *Kα* radiation (λ = 0.71073 Å). Biagioniite was found to be monoclinic, with *a* = 11.0895(9), *b* = 14.3124(11), *c* = 7.9352(6) Å, β = 96.230(8)°, *V* = 1252.02(17) $Å^3$ and Z = 8. The analysis of the systematic absences (*h*0*l*: *l* = 2*n* and 00*l*: *l* = 2*n*) led to the choice of the space groups

Pc and *P*2/*c*. Although the statistical tests on the distribution of |*E*| values (|E^2-1| = 0.812) indicated the absence of an inversion centre, suggesting the choice of the space group *Pc*, the structure was preliminarily solved in the *P*2/*c* space group. A residual R_1 = 0.18 value was quickly achieved. However, the preliminary structural model obtained indicated a large atomic disorder. The structure model was subsequently optimized, and an ordered model was sought, but no improvement in *R* could be achieved. At this point, a thorough analysis of the structure (essentially based upon the observation of the very large atomic displacement parameters for particular atoms) suggested that some symmetry element of the *P*2/*c* space group should be removed. The reflection and atomic position data sets were then adapted to the *Pc* space group (showing the same reflections conditions) and the structure refined. After several cycles, an ordered solution with full site occupancies was finally determined by carefully removing atoms with low site occupancies and/or non-realistic distances with neighbouring atoms and adding significant positions found in the difference Fourier syntheses. The structure could be smoothly refined in *Pc* without any damping factor or restrictions by the program SHELXL (Sheldrick, 2008). The occupancy of all the sites was left free to vary (Tl vs. □; Sb vs. □; S vs. □) but all the positions were found to be fully occupied. Neutral scattering curves for Ag, As and S were taken from the *International Tables for X-ray Crystallography* (Wilson, 1992). At the last stage, with anisotropic atomic displacement parameters for all the atoms and no constraints, the residual value settled at R_1 = 0.0243 for 2655 observed reflections [2σ(*I*) level] and 182 parameters and at R_1 = 0.0315 for all 4520 independent reflections.

It is worth of note that the acentric structural model we obtained does not show high values in the correlation matrix between pairs of atoms which are equivalent in the centrosymmetric space group *P*2/*c*. To test whether the acentric model is to be preferred to the centric one we also test the presence of twinning by inversion in the non-centrosymmetric

structure refinement. Indeed, as it is well known, a centrosymmetric structure that is refined as non-centrosymmetric will show a twin scale factor, equivalent to the Flack parameter in the case of inversion twinning (Flack *et al.*, 2006; Müller *et al.*, 2006), that refines to 50% within analytical uncertainty. We found the racemic twin-component scale factor refined to 0.09(2), consistent with a highly asymmetrical distribution of the enantiomorphic components and indicating the acentric model as the right choice.

Experimental details and *R* indices are given in Table 2. Fractional atomic coordinates and atomic displacement parameters are reported in Table 3. Bond distances are given in Table 4. CIF is deposited with the Principal Editor of Mineralogical Magazine at http://www.minersoc.org/pages/e_journals/dep_mat.html.

X-ray powder diffraction data (Table 5) were collected with an Oxford Diffraction Excalibur PX Ultra diffractometer fitted with a 165 mm diagonal Onyx CCD detector and using copper radiation (Cu *K*α, λ = 1.54138 Å). The least squares refinement gave the following values: a = 11.0999(9), b = 14.273(1), c = 7.9323(7) Å, β = 96.29(1)°, and V = 1249.1(1) Å^3.

DESCRIPTION OF THE STRUCTURE AND DISCUSSION

The structure of biagioniite projected down [001] is reported in Figure 2. It is isostructural with dervillite, Ag_2AsS_2 (Bindi *et al.*, 2013). Enlarged Figure 3 permits to distinguish $Tl_4(Sb_2)_2S_6$ ribbons parallel to [001], stacked along [010], to form undulated layers along [100]. These layers are separated by one-atom-thick Tl_4S_2 layer. Noteworthy, there are two Sb–Sb pairs, Sb1–Sb3 (2.843 Å) and Sb2–Sb4 (2.830 Å).

Figure 4 represents the coordination of these pairs. Coordination of each pair with four S atoms corresponds to a hemi-octahedron cut along a symmetry plane (through two opposite

edges of the cube – Fig. 5). Two neighboring hemi-octahedra brought closer permit to rebuild a single octahedron.

In the $Tl_4(Sb_2)_2S_6$ ribbon-layer, Tl1 and Tl3 exhibit a tetrahedral coordination with S, whereas the coordination is triangular for Tl4 and Tl5. Nevertheless, the coordination environment for Tl4 and Tl5 is completed by additional short Tl-Sb bonds (Tl5–Sb1 = 3.067 Å and Tl4–Sb4 = 3.175 Å).

Figure 6 shows the coordination of Tl atoms of the Tl_4S_2 layer. There is a central zig-zag row of tetrahedral Tl atoms, flanked by two stripes of triangular Tl, and then two stripes of linear Tl. Contrary to the $Tl_4(Sb_2)_2S_6$ ribbon-layer (see below), here there is linear Tl on one mirror position, and tetrahedral Tl along the second mirror position. It is worth noting the linear coordination of Tl7. To the best of our knowledge, biagioniite seems to be the first example of a natural chalcogenide showing Tl in linear coordination. For a review of Tl chalcogenides see Makovicky (2018).

In Figure 7, the Sb_2 pairs have been replaced by a single atom (G) at their gravity center, and an anionic vacancy (□) has been added. One $Tl_4(Sb_2)_2S_6$ ribbon (now $Tl_4G_2S_6□_2$) has been selected. Projection of this ribbon (Fig. 8) shows that it is a distorted derivative of the PbS structure. The Pb_6S_8 ideal ribbon (Fig. 9) is parallel to [310], two-atom-thick, and three-octahedron large. Junction between two ribbons along [010] (mirror in the structure, with a shift along *c*, to preclude S−S short bond in the interface) corresponds to (131) of PbS. The two sides of such a junction (the two different mirror positions) have the same topology.

Bond valence calculations (Table 6) have been computed on the basis of the following bond parameters: $R_{Sb,S}$ = 2.45 (Brese and O'Keeffe, 1991), $R_{Tl,S}$ = 2.55 (Biagioni *et al.*, 2014) and $R_{Sb,Sb}$ = 2.82 (O'Keeffe and Brese, 1992). Tl atoms are overbonded (bond valence from 1.11 up to 1.36 valence unit, v.u.), but we have not considered in the computation the presence of minor Ag disordered at the Tl positions, although it would be very minor. Sb-Sb

bond lengths (2.830 and 2.843 Å) quite agree with $R_{Sb,Sb}$ corresponding to one v.u.; nevertheless, Sb atoms are underbonded varying from 2.31 to 2.57 v.u. The overall bond-valence sum of S, 15.95 v.u., is very close to the theoretical value (16 v.u.). These results may be due to uncertainty in the positions of some S atoms: a small shift closer to Sb atoms would reduce Sb underbonding together with Tl overbonding, without significant change of S bond-valence sum.

The presence of dimeric $[Sb_2S_4]^{4-}$ ions with a central Sb–Sb bond in biagioniite could bring to write the formula as $[Tl^{+1}]_4[Sb_2]^{4+}[S^{2-}]_4$. However, it is difficult to analyze such polycationic compounds in strict bond-valence terms, since the electronegativity of such elements lies between that of common cations and common anions. The weak Tl–Sb bonds in biagioniite are good examples of the "anionic" behavior, which could be explained through dative donation of the Sb lone pair to the closed-shell d^{10} Tl cations. On the contrary, in dervillite, short Ag-As bonds are lacking (Bindi *et al.*, 2013).

Tl_2SbS_2 has been never described either in nature or as synthetic compound. Actually, the experimental $TlSbS_2$–Tl section includes three ternary compounds, namely Tl_2SbS_2, Tl_4SbS_2 and Tl_5SbS_2. The former two compounds melt congruently at 613 and 683 K, whereas the latter one decomposes by peritectic reaction at 663 K (Jafarov *et al.*, 2016). But, in fact, Tl_2SbS_2 compound has been found to be Tl_3SbS_3+Sb two-phase mixture instead of a single, independent chemical compound. Such a S−deficient formula for biagioniite indicates its formation at Hemlo at low $f(S_2)$, in accordance to its association with stibarsen, SbAs, aurostibite, $AuSb_2$, and criddleite, $TlAg_2Au_3Sb_{10}S_{10}$ (also S−deficient).

Acknowledgments

The manuscript took advantage from the review of Federica Zaccarini, Stuart Mills, and an anonymous reviewer. The research was funded by MIUR-PRIN2017, project

"TEOREM deciphering geological processes using Terrestrial and Extraterrestrial ORE Minerals", prot. 2017AK8C32 (PI: Luca Bindi).

REFERENCES

Biagioni, C., Bindi, L., Nestola, F., Cannon, R., Roth, P. and Raber, T. (2016) Ferrostalderite, $CuFe_2TlAs_2S_6$, a new member of the routhierite new mineral from Lengenbach, Switzerland: occurrence, crystal structure, and emphasis on the role of iron in sulfosalts. *Mineralogical Magazine*, **80**, 175–186.

Biagioni, C., Bonaccorsi, E., Moëlo, Y., Orlandi, P., Bindi, L., D'Orazio, M. and Vezzoni, S. (2014) Mercury-arsenic sulfosalts from the Apuan Alps (Tuscany, Italy). II. Arsiccioite, $AgHg_2TlAsS_6$, a new mineral from the Monte Arsiccio mine: Occurrence, crystal structure and crystal chemistry of the routhierite isotypic series. *Mineralogical Magazine*, **78**, 101–117.

Biagioni, C., D'Orazio, M., Lepore, G.O., d'Acapito, F. and Vezzoni, S. (2017) Thallium-rich rust scales in drinkable water distribution systems: A case study from northern Tuscany, Italy. *Science of the Total Environment*, **587-588**, 491–501.

Biagioni, C., D'Orazio, M., Vezzoni, S., Dini, A. and Orlandi, P. (2013) Mobilization of Tl-Hg-As-Sb-(Ag,Cu)-Pb sulfosalt melts during low-grade metamorphism in the Alpi Apuane (Tuscany, Italy). *Geology*, **41**, 747–750.

Bindi, L. and Biagioni, C. (2018) A crystallographic excursion in the extraordinary world of minerals: The case of Cu- and Al-rich sulfosalts. *Acta Crystallographica*, **B74**, 527–538.

Bindi, L., Biagioni, C., Raber, T., Roth, P. and Nestola, F. (2015) Ralphcannonite, $AgZn_2TlAs_2S_6$, a new mineral of the routhierite isotypic series from Lengenbach, Binn Valley, Switzerland. *Mineralogical Magazine*, **79**, 1089–1098.

Bindi, L., Nestola, F., De Battisti, L. and Guastoni, A. (2013) Dervillite, Ag_2AsS_2, from Lengenbach quarry, Binn Valley, Switzerland: occurrence and crystal structure. *Mineralogical Magazine*, **77**, 3105–3112.

Bindi, L., Nestola, F., Guastoni, A., Peruzzo, L., Ecker, M. and Carampin, R. (2012a) Raberite, $Tl_5Ag_4As_6SbS_{15}$, a new Tl-bearing sulfosalt from Lengenbach quarry, Binn Valley, Switzerland: description and crystal structure. *Mineralogical Magazine*, **76**, 1153–1163.

Bindi, L., Nestola, F., Graeser, S., Tropper, P. and Raber, T. (2015) Eckerite, Ag_2CuAsS_3, a new Cu-bearing sulphosalt from Lengenbach quarry, Binn valley, Switzerland: description and crystal structure. *Mineralogical Magazine*, **79**, 687–694.

Bindi, L., Nestola, F., Guastoni, A., Zorzi, F., Peruzzo, L. and Raber, T. (2012b) Te-rich canfieldite, $Ag_8Sn(S,Te)_6$, from Lengenbach quarry, Binntal, Canton Valais, Switzerland: Occurrence, description and crystal structure. *Canadian Mineralogist*, **50**, 111–118.

Brese, N.E. and O'Keeffe, M. (1992) Bond-valence parameters for solids. *Acta Crystallographica*, **B47**, 192–197.

Flack, H.D., Bernardinelli, G., Clemente, D.A., Lindenc, A. and Spek, A.L. (2006) Centrosymmetric and pseudo-centrosymmetric structures refined as non-centrosymmetric. *Acta Crystallographica*, **B62**, 695–701.

Harris, D.C. (1989) The mineralogy and geochemistry of the Hemlo gold deposit, Ontario. *Geological Survey of Canada, Economic Geology Report*, 38, 1–88.

Jafarov, Y.I., Ismayilova, S.A., Aliev, Z.S., Imamaliyeva, S.Z., Yusibov, Y.A. and Babanly, M.B. (2016) Experimental study of the phase diagram and thermodynamic properties of the Tl-Sb-S system. *Calphad*, **55**, 231–237.

Makovicky, E. (2018) Modular crystal-chemistry of thallium sulfosalts. *Minerals*, **8**, 478.

Müller, P., Herbst-Irmer, R., Spek, A.L., Schneider, T.R. and Sawaya, M.R. (2006) Crystal structure refinement, a crystallographer's guide to SHELXL. Oxford University Press (for IUCr), London, 213 p.

O'Keeffe, M. and Brese, N.E. (1992) Bond-valence parameters for anion-anion bonds in solids. *Acta Crystallographica*, **B48**, 152–154.

Sheldrick, G.M. (2008) A short history of SHELX. *Acta Crystallographica*, **A64**, 112–122.

Tomkins, A.G., Pattison, D.R.M. and Zaleski, E. (2004) The Hemlo Gold deposit, Ontario: An example of melting and mobilization of a precious metal-sulfosalt assemblage during amphibolites facies metamorphism and deformation. *Economic Geology*, **88**, 1063–1084.

Wilson, A.J.C., Ed. (1992) *International Tables for Crystallography*, Volume C: Mathematical, physical and chemical tables. Kluwer Academic, Dordrecht, NL.

TABLE AND FIGURE CAPTIONS

TABLE 1 – Electron microprobe analysis (wt% of elements) of biagioniite.

	Mean	Range
Ag	3.52	3.35 – 3.77
Tl	65.12	64.58 – 65.79
Sb	20.22	19.65 – 21.08
S	10.80	10.02 – 11.23
total	99.66	99.09 – 100.16

TABLE 2 – Crystallographic data and refinement parameters for biagioniite.

Crystal data	
Formula	Tl_2SbS_2
Crystal size (mm)	0.040 × 0.050 × 0.065
Form	block
Colour	black
Crystal system	monoclinic
Space group	*Pc* (#7)
a (Å)	11.0895(9)
b (Å)	14.3124(11)
c (Å)	7.9352(6)
β (°)	96.230(8)
V (Å^3)	1252.02(17)
Z	8
Data collection	
Instrument	Bruker D8 Venture
Radiation type	Mo*K*α (λ = 0.71073)
Temperature (K)	293(3)
Detector to sample distance (cm)	6
Number of frames	1248
Measuring time (s)	30
Maximum covered 2θ (°)	74.98
Absorption correction	multi-scan
Collected reflections	20833
Unique reflections	4520
Reflections with $F_o > 4\sigma(F_o)$	2655
R_{int}	0.0321
R_σ	0.0424
Range of *h, k, l*	$-16 \le h \le 16$, $-21 \le k \le 21$, $-13 \le l \le 13$
Refinement	

Refinement	Full-matrix least squares on F^2
Final R_1 [$F_o > 4\sigma(F_o)$]	0.0243
Final R_1 (all data)	0.0315
Number refined parameters	182
GoF	0.939
$\Delta\rho_{max}$ (e Å^{-3})	1.72
$\Delta\rho_{min}$ (e Å^{-3})	-1.57

TABLE 3 – Atoms, fractional atom coordinates (Å), and atomic displacement parameters (Å^2) for biagioniite.

atom	*x*/*a*	*y*/*b*	*z*/*c*	U_{eq}
Tl1	0.23733(13)	0.59615(8)	0.42312(14)	0.0344(3)
Tl2	0.04141(14)	0.91367(9)	0.72629(15)	0.0437(4)
Tl3	0.69297(12)	0.90702(8)	0.12240(13)	0.0299(3)
Tl4	0.35736(13)	0.89299(8)	0.62921(17)	0.0356(3)
Tl5	0.56511(13)	0.60615(8)	0.89568(17)	0.0355(3)
Tl6	0.96143(15)	0.79027(10)	0.30728(18)	0.0526(4)
Tl7	0.8383(2)	0.49262(12)	0.6517(2)	0.0838(7)
Tl8	0.96092(16)	0.68618(11)	0.8476(2)	0.0713(5)
Sb1	0.31287(16)	0.68477(11)	0.9379(2)	0.0143(4)
Sb2	0.61774(17)	0.68126(12)	0.3516(2)	0.0167(4)
Sb3	0.30962(17)	0.83097(11)	0.1799(2)	0.0155(4)
Sb4	0.62590(17)	0.82160(12)	0.6039(2)	0.0157(4)
S1	0.1528(7)	0.5806(4)	0.0502(9)	0.0188(15)
S2	0.7909(7)	0.9183(5)	0.5002(8)	0.0177(14)
S3	0.1927(7)	0.7465(4)	0.6551(8)	0.0162(14)
S4	0.7352(8)	0.7510(5)	0.8912(8)	0.0229(17)
S5	0.8479(7)	0.6293(4)	0.4144(9)	0.0191(15)
S6	0.5150(7)	0.5673(5)	0.5200(9)	0.0237(17)
S7	0.0903(7)	0.8956(5)	0.1036(8)	0.0202(15)
S8	0.4270(7)	0.9350(4)	0.0130(9)	0.0179(14)

TABLE 4 – Selected bond distances (Å) for biagioniite.

Tl1-S3	2.909(6)	Tl5-S6	2.750(7)	Sb1-S1	2.552(8)
Tl1-S1	2.916(7)	Tl5-S4	2.805(8)	Sb1-S3	2.635(6)
Tl1-S1	3.014(7)	Tl5-S6	3.024(7)	Sb1-Sb3	2.843(2)
Tl1-S6	3.119(8)	Tl5-Sb1	3.067(2)	<Sb1-S>	2.677
<Tl1-S>	2.990	<Tl5-S>	2.912		
Tl2-S7	2.967(7)	Tl6-S7	2.726(7)	Sb2-S6	2.465(8)

Tl2-S7	2.995(6)	Tl6-S5	2.802(7)	Sb2-S5	2.653(8)
Tl2-S3	3.011(6)	Tl6-S2	3.148(7)	Sb2-Sb4	2.830(3)
Tl2-S2	3.140(7)	<Tl6-S>	2.892	<Sb2-S>	2.649
<Tl2-S>	3.028				
Tl3-S2	2.932(7)	Tl7-S5	2.712(7)	Sb3-S8	2.458(7)
Tl3-S4	2.960(7)	Tl7-S5	2.725(7)	Sb3-S7	2.612(7)
Tl3-S8	3.010(7)	<Tl7-S>	2.719	Sb3-Sb1	2.843(2)
Tl3-S2	3.080(6)			<Sb3-S>	2.638
<Tl3-S>	2.996				
Tl4-S8	2.768(7)	Tl8-S4	2.726(9)	Sb4-S2	2.504(8)
Tl4-S3	2.802(7)	Tl8-S1	2.942(7)	Sb4-S4	2.663(7)
Tl4-S8	3.118(7)	Tl8-S3	3.246(7)	Sb4-Sb2	2.830(3)
<Tl4-S>	2.896	<Tl8-S>	2.971	<Sb4-S>	2.666

TABLE 5 – Observed and calculated X-ray powder diffraction data for biagioniite.

			1		**2**	
h	*k*	*l*	d_{obs}	I_{est}	d_{calc}	I_{calc}
1	2	1	4.65	10	4.6463	12
2	1	1	-	-	4.1219	9
-2	2	1	3.98	20	3.9678	23
-1	3	1	3.89	15	3.9002	19
-1	0	2	3.85	20	3.8485	22
0	1	2	3.79	60	3.8024	67
1	3	1	3.75	15	3.7601	23
2	2	1	-	-	3.6885	14
3	0	0	3.68	40	3.6747	40
2	3	0	-	-	3.6073	8
1	0	2	-	-	3.5921	9
0	4	0	3.58	20	3.5781	18
3	1	0	3.56	100	3.5592	100
1	1	2	3.48	40	3.4840	47
0	2	2	-	-	3.4543	26
1	4	0	3.39	20	3.4033	24
-1	2	2	-	-	3.3894	15
-2	0	2	-	-	3.3862	25
-2	3	1	3.37	75	3.3724	81
3	2	0	3.27	35	3.2689	36
0	4	1	3.24	20	3.2585	23
1	2	2	-	-	3.2103	19
-1	4	1	3.16	40	3.1637	37
-3	2	1	-	-	3.1286	10
1	4	1	3.08	40	3.0875	39
0	3	2	3.03	60	3.0398	62
2	1	2	-	-	2.9873	11
-2	4	1	-	-	2.8618	15

2	2	2	-	-	2.8093	9
-3	1	2	2.795	20	2.7924	19
-2	3	2	-	-	2.7613	8
2	4	1	-	-	2.7515	19
3	0	2	2.555	20	2.5539	25
-4	2	1	-	-	2.5216	12
3	1	2	2.515	20	2.5142	17
3	4	1	-	-	2.3855	9
4	2	1	-	-	2.3753	8
-4	3	1	-	-	2.3461	14
-2	2	3	2.342	30	2.3434	29
0	5	2	-	-	2.3167	15
3	5	0	-	-	2.2582	19
-3	4	2	2.228	30	2.2279	26
1	6	1	-	-	2.2220	14
1	3	3	-	-	2.2125	17
-1	4	3	2.116	20	2.1153	22
-5	2	1	2.089	30	2.0905	31
2	6	1	-	-	2.0864	8
3	4	2	-	-	2.0787	14
4	4	1	-	-	2.0593	15
5	1	1			2.0449	9
0	0	4	-	-	1.9721	9
-1	7	1	-	-	1.9574	15
2	4	3	-	-	1.9223	9
-2	7	1	-	-	1.8791	12
-3	6	2	-	-	1.8285	9
-5	1	3	-	-	1.7739	9
-1	6	3	-	-	1.7647	9
-6	5	2	-	-	1.4864	8

1 = observed diffraction pattern; 2 = calculated diffraction pattern obtained with the atom coordinates and occupancies reported in Table 3 (only reflections with $I_{rel} \geq 8$ are listed).

TABLE 6 – Bond-valence sums for biagioniite.

Tl1	1.25	S1	1.76
Tl2	1.11	S2	1.86
Tl3	1.21	S3	1.99
Tl4	1.28	S4	2.02
Tl5	1.36	S5	2.35
Tl6	1.33	S6	2.04
Tl7	1.27	S7	1.89
Tl8	1.12	S8	2.04
Sb1	2.31		
Sb2	2.51		
Sb3	2.57		
Sb4	2.40		

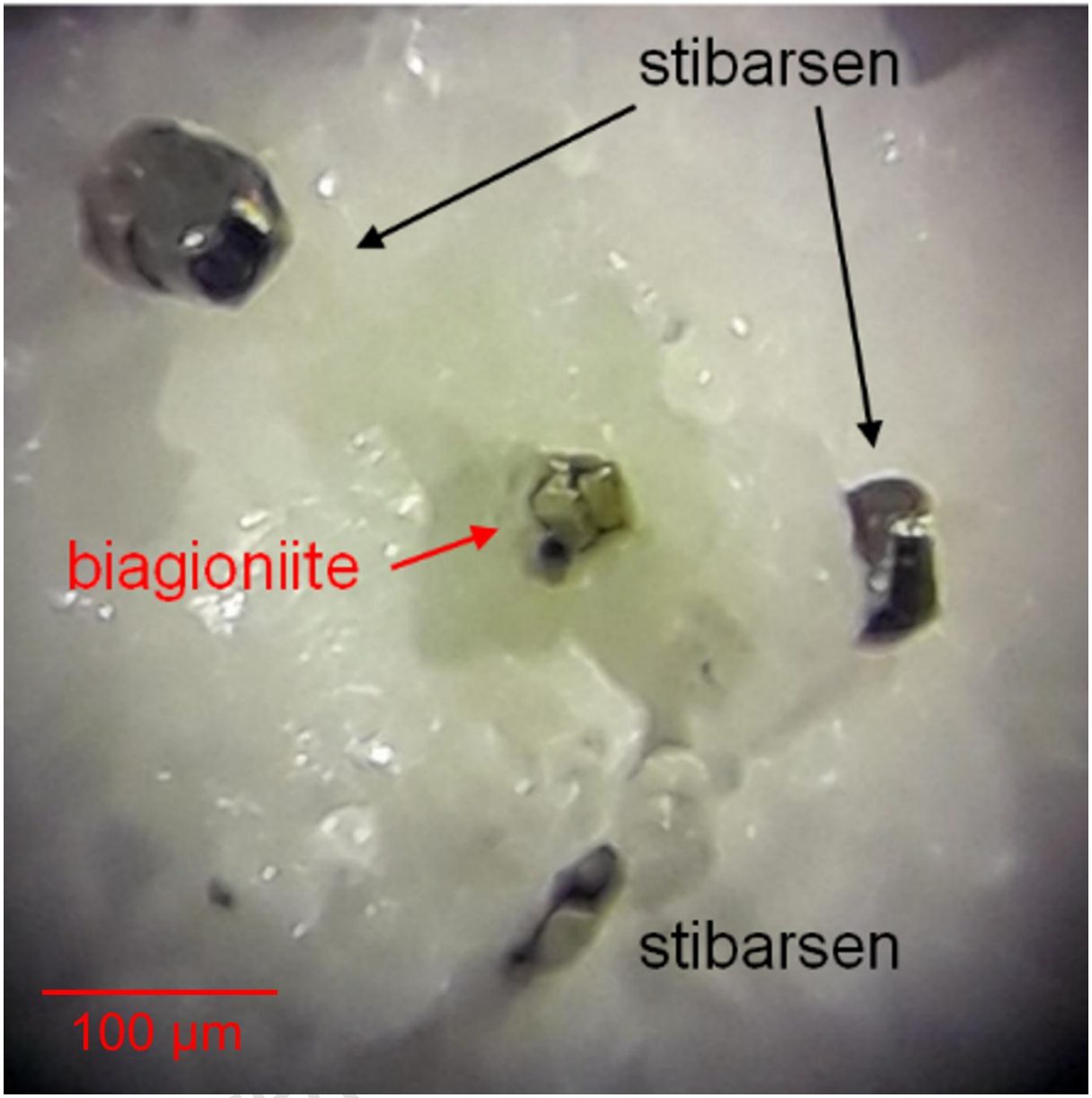

FIGURE 1 – Incident-light image of biagioniite associated with stibarsen on a calcite matrix.

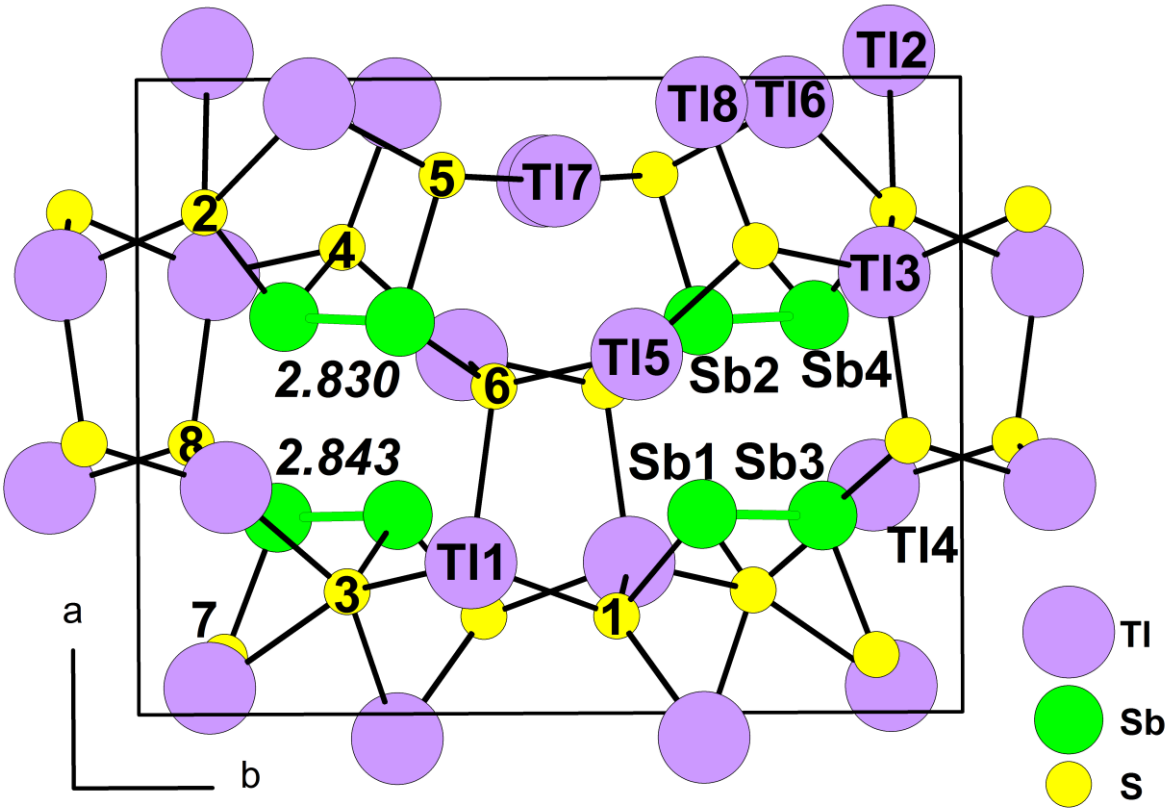

FIGURE 2 – The crystal structure of biagioniite down [001]: unit-cell content, atoms labels and Sb–Sb bond lengths (Å). Tl, Sb and S atoms are given as purple, green and yellow circles, respectively.

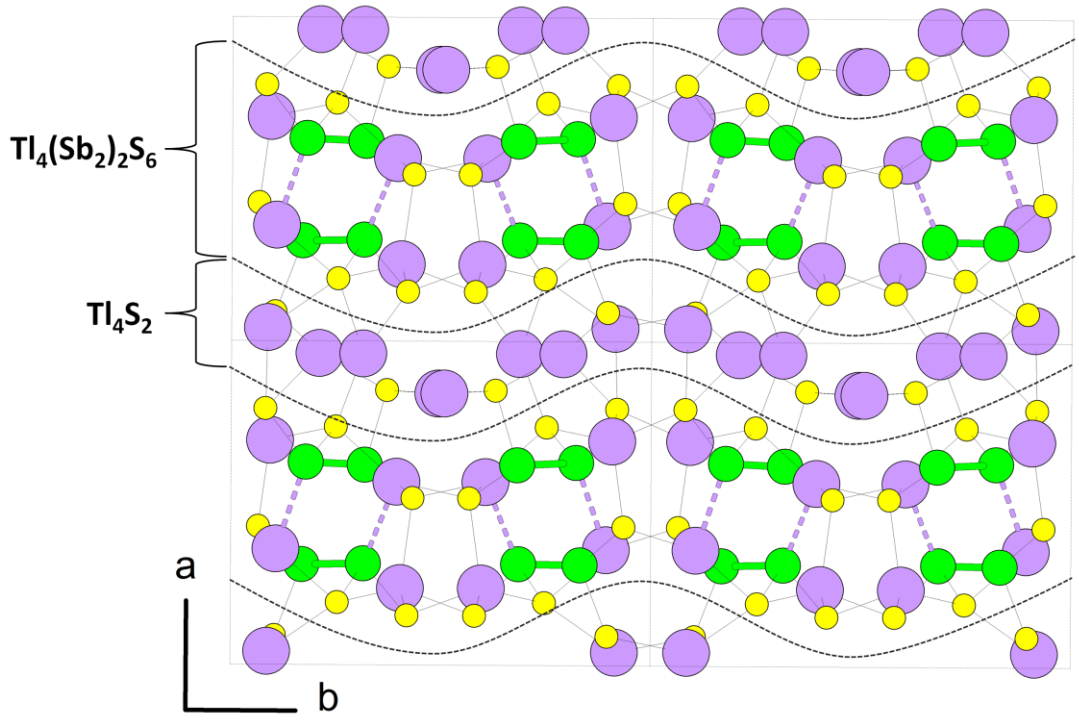

FIGURE 3 – Biagioniite: 2*a* × 2*b* cell. $Tl_4(Sb_2)_2S_6$ ribbons parallel to [001], stacked along [010], form undulated layers along [100]. These layers are separated by one-atom-thick layer Tl_4S_2.

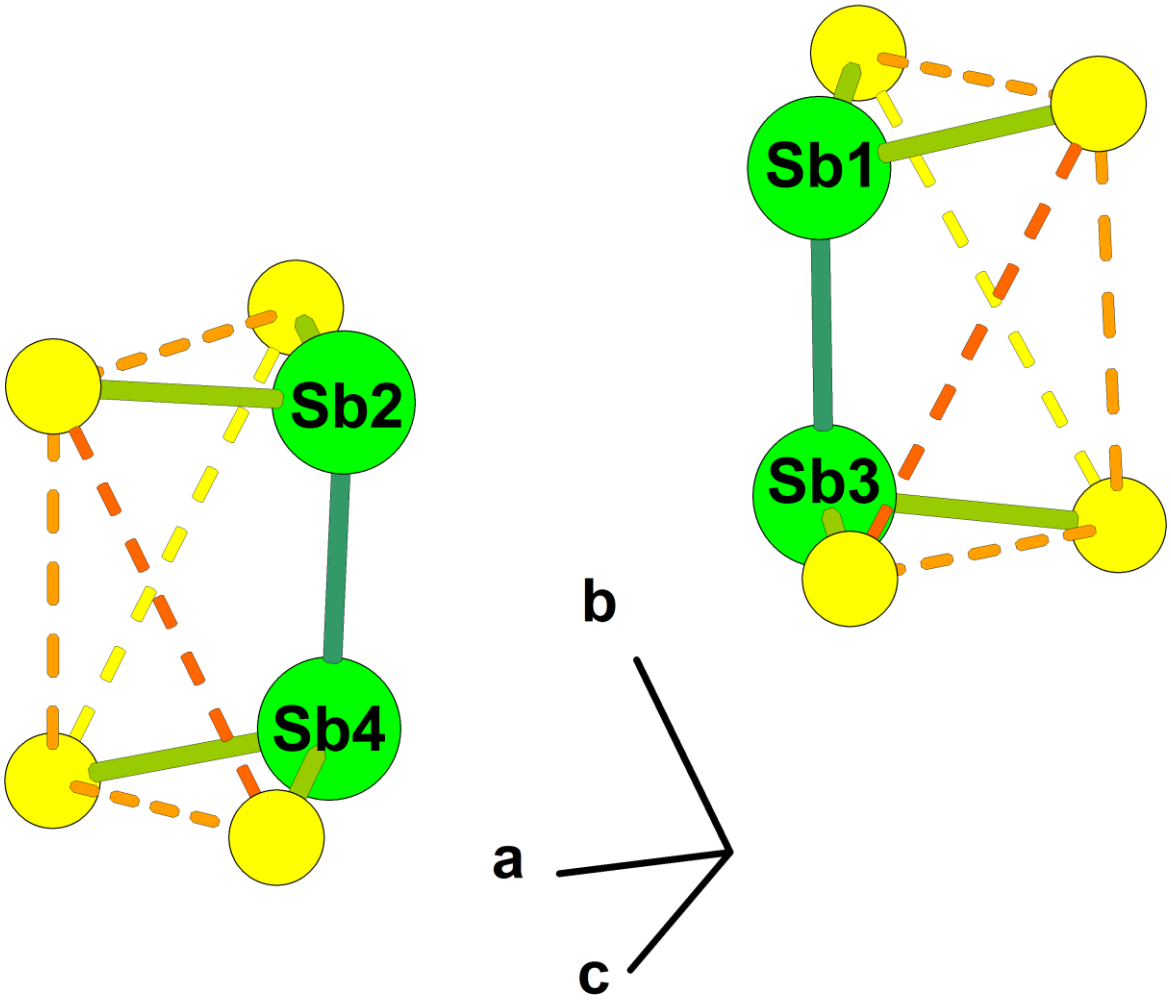

FIGURE 4 – Coordination of the Sb pairs with S atoms.

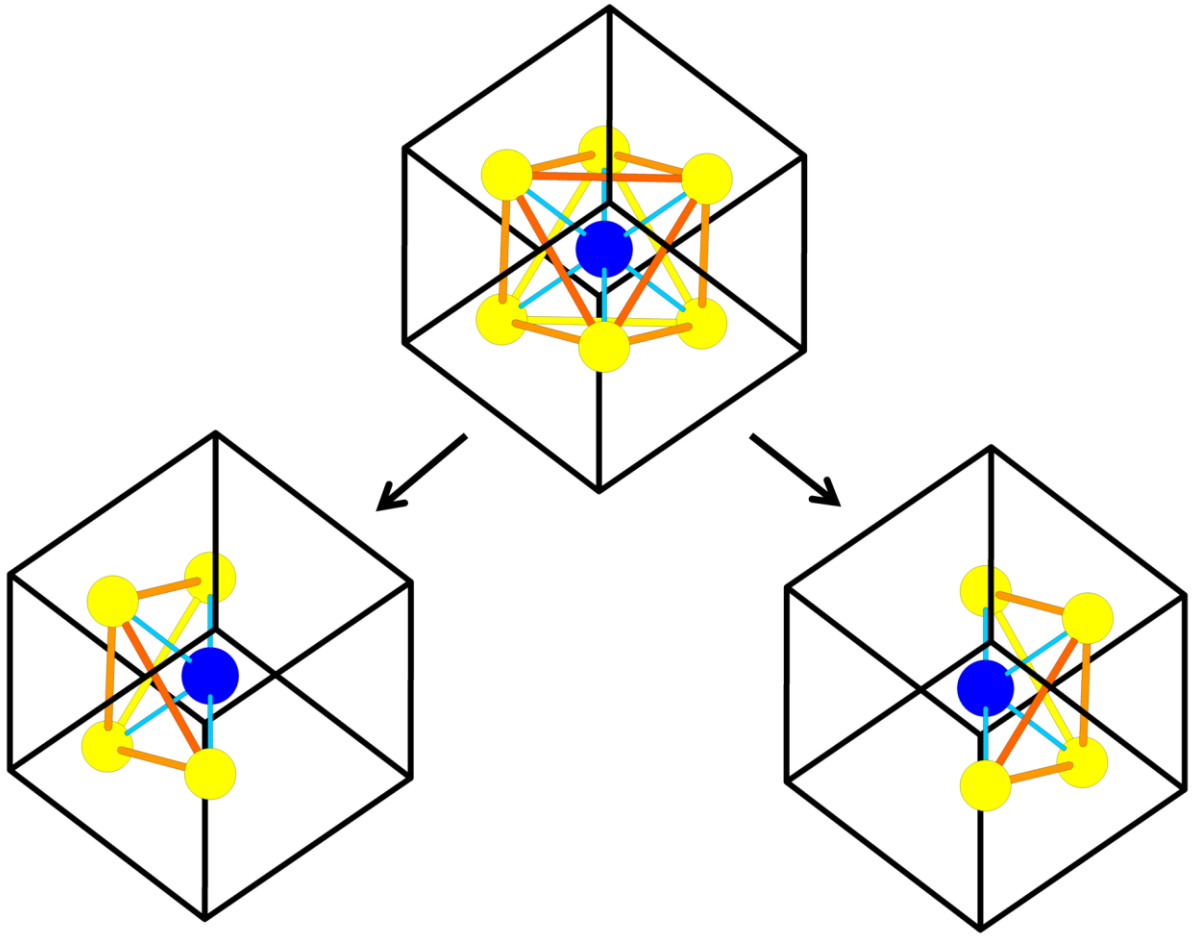

FIGURE 5 – Coordination of each Sb pair (down, reduced to a central blue atom) with four S atoms corresponding to a hemi-octahedron cut along a symmetry plane (through two opposite edges of the cube). Two neighboring hemi-octahedra brought closer permit to rebuild the octahedron (above).

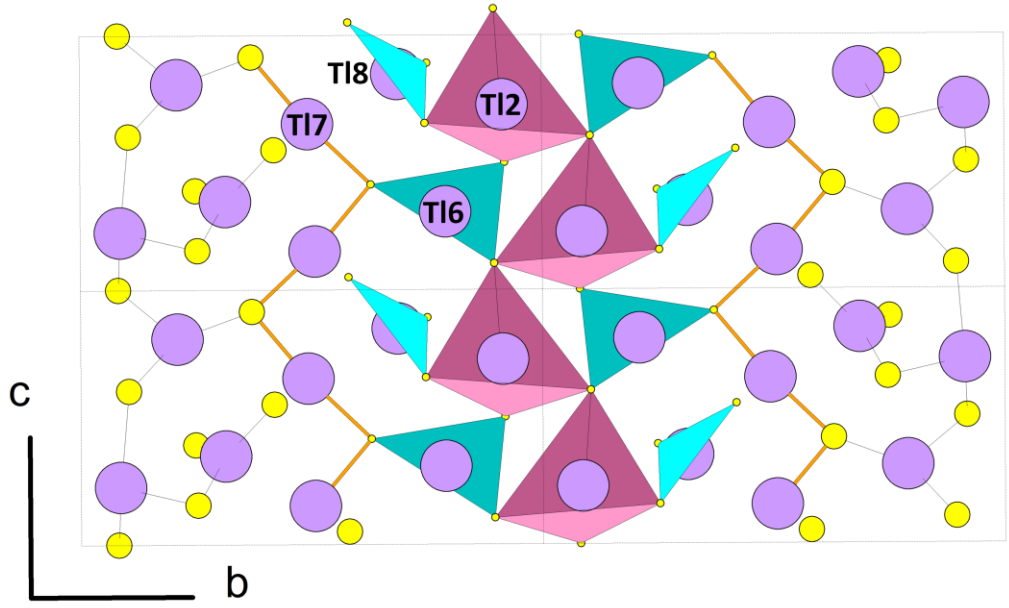

FIGURE 6 – Coordination of Tl atoms in the Tl_4S_2 layer in the structure of biagioniite. Tl3: tetrahedral; Tl6 and Tl8: triangular; Tl7: linear.

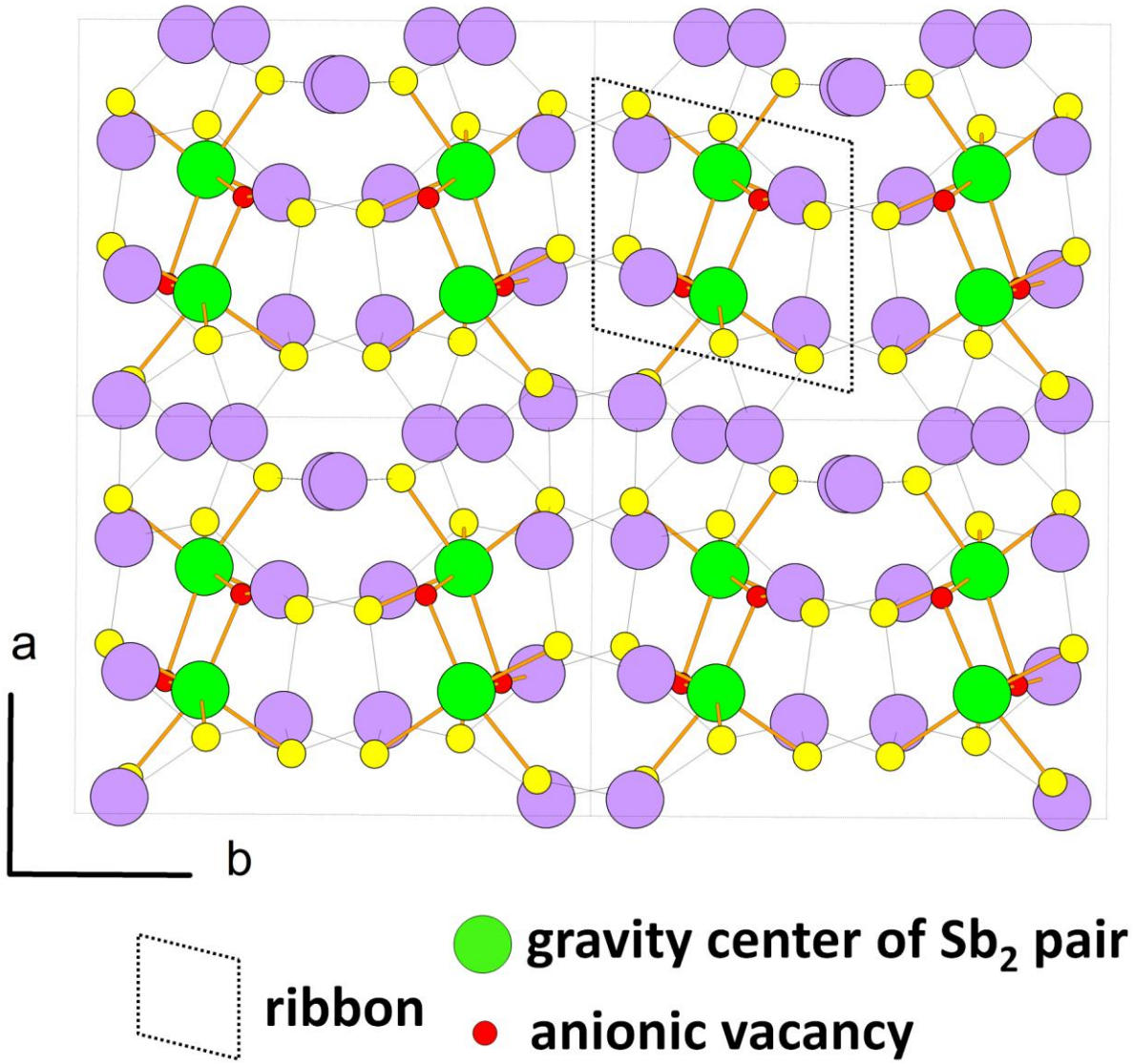

FIGURE 7 – Sb_2 pairs have been replaced by a single atom (G, green) at their gravity center, and an anionic vacancy (□, red) has been added. One $Tl_4(Sb_2)_2S_6$ ribbon (now $Tl_4G_2S_6□_2$) has been selected.

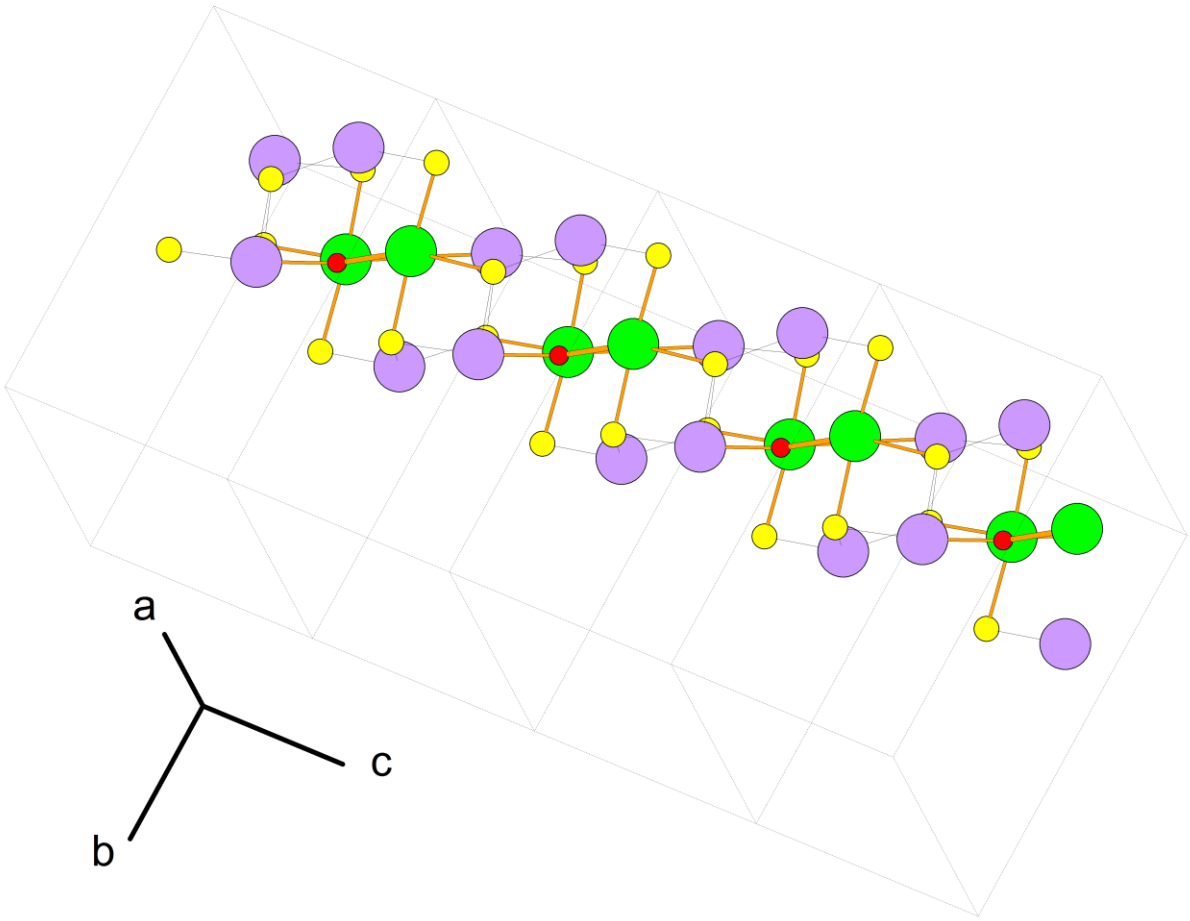

FIGURE 8 – One $Tl_4G_2S_6\square_2$ ribbon in the crystal structure of biagioniite can be described as a distorted derivative of PbS structure.

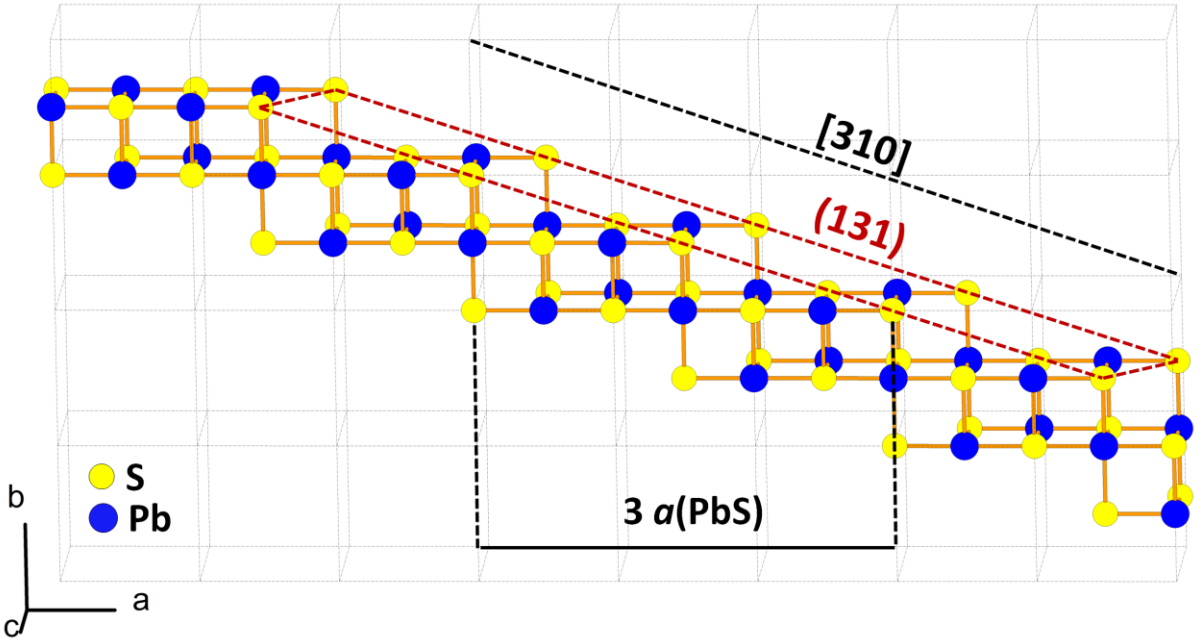

FIGURE 9 – A Pb_6S_8 ideal ribbon parallel to [310], two-atom-thick, and three-octahedra large. Junction between two ribbons in the structure of biagioniite along [010] corresponds to (131) of PbS.